Journal of the Geological Society, London, Vol. **160**, 2003, pp. 881–894. Printed in Great Britain.

The structural and diagenetic evolution of injected sandstones: examples from the Kimmeridgian of NE Scotland

R. JONK[1], D. DURANTI[1], J. PARNELL[1], A. HURST[1] & A. E. FALLICK[2]
[1]*Department of Geology and Petroleum Geology, University of Aberdeen, Aberdeen AB24 3UE, UK*
(e-mail: r.jonk@abdn.ac.uk)
[2]*Scottish Universities Environmental Research Centre, East Kilbride, Glasgow G75 0QF, UK*

Abstract: Injected sandstones occurring in the Kimmeridgian of NE Scotland along the bounding Great Glen and Helmsdale faults formed when basinal fluids moved upward along the fault zones, fluidizing Oxfordian sands encountered at shallow depth and injecting them into overlying Kimmeridgian strata. The orientation of dykes, in addition to coeval faults and fractures, was controlled by a stress state related to dextral strike-slip along the bounding fault zones. Diagenetic studies of cements allow the reconstruction of the fluid flow history. The origin of deformation bands in sandstone dykes and sills was related to the contraction of the host-rocks against dyke and sill walls following the initial stage of fluidized flow, and these deformation bands are the earliest diagenetic imprint. Early non-ferroan calcite precipitated in injection structures at temperatures between 70 and 100 °C, indicating that it precipitated from relatively hot basinal fluids that drove injection. Coeval calcite-filled fractures show similar temperatures, suggesting that relatively hot fluids were responsible for calcite precipitation in any permeable pathway created by dextral simple shear along the faults. During progressive burial, percolating sea water was responsible for completely cementing the still relatively porous injected sandstones with a second generation of ferroan calcite, which contains fluid inclusions with homogenization temperatures below 50 °C. During this phase, depositional host sandstones were also cemented.

Keywords: Kimmeridgian, sandstone dykes, carbonates, cements, deformation.

Sandstone dykes and sills have been reported in the geological literature for over a hundred years (Murchison 1827; Diller 1890; Newsome 1903). Initially they were treated as geological curiosities, but during the past 10 years (Jolly & Lonergan 2002) it has been recognized that injected sandstones, as opposed to those formed by passive infilling of open cracks (Richter 1966), are a common structure in sedimentary basins. In particular, large-scale injected sandstones occurring in the Tertiary deposits of the North Sea basin have been described (Jenssen *et al*. 1993; Dixon *et al*. 1995; Duranti *et al*. 2002). Contemporaneous (hydraulic) fracturing and sand injection can often be demonstrated (Lonergan & Cartwright 1999; Cosgrove 2001) and their combined impact on controlling past and present fluid flow patterns within generally low-permeability host rocks may be substantial. Injected sands have a major effect on fluid flow during their formation as fluidized flows (Jolly & Lonergan 2002), but critical in assessing their impact on long-term fluid flow is to assess whether sandstone injections will behave either as barriers (when cemented) or as conduits (when uncemented). When cemented, it is critical to understand when cementation took place, so as to understand when conduits may change into barriers. Outcrop studies of injected sandstones have been devoted to geometrical analysis of dykes and sills (e.g. Winslow 1983; Huang 1988; Jolly *et al*. 1998). Outcrop-based studies combined with diagenetic studies are seemingly absent in the literature. A study of the diagenetic features is an essential component in evaluating fluid flow. Moreover, injected sandstones are often treated in isolation, without analysing contemporaneous fractures that occur in the vicinity of injections. In this study we present field observations combined with diagenetic studies and reconstruct the events that led to sand injection and the processes that took place within dykes and sills following injection. The area of study is the onshore Kimmeridgian of NE Scotland, in which carbonate-cemented injected sandstones and carbonate-cemented fractures occur.

Geological setting of the studied area

Exposures of Upper Jurassic sediments near Helmsdale, Eathie and Port an Righ are downfaulted to the SE against granites, gneisses and Devonian sedimentary rocks to the NW (Fig. 1). All studied exposures are located along the fault-bounded north-western margin of the Inner Moray Firth Basin (Roberts *et al*. 1990). Cores from boreholes indicate that the Inner Moray Firth has been a sedimentary basin since the Devonian (Bird *et al*. 1987). The apparent lack of crustal thinning beneath the Inner Moray Firth (Donato & Tully 1981) makes the basin different from other North Sea basins with a more extensional origin. The Great Glen and the Helmsdale faults, along which the Jurassic outliers of Eathie and Helmsdale, respectively, are found, show a complex history of movements. The Great Glen Fault has long been recognized as a strike-slip fault (McQuillin *et al*. 1982). The consensus is that overall relative dextral movement of few tens of kilometres has occurred since the Devonian (Speight & Mitchell 1979). McQuillin *et al*. (1982) stated that the Inner Moray Firth Basin developed as a dextral pull-apart along the Great Glen Fault. Barr (1985) derived similar conclusions following 3D palinspastic restoration of the basin. Although different views on the post-Devonian phases of movement exist (Bird *et al*. 1987; Roberts *et al*. 1990; Thomson & Underhill 1993; Underhill & Brodie 1993; McBride 1994), the view of McQuillin *et al*. (1982) is generally accepted. During the late Jurassic, the Helmsdale Fault and Great Glen Fault accommodated dip-slip extension related to rifting. The early Cretaceous

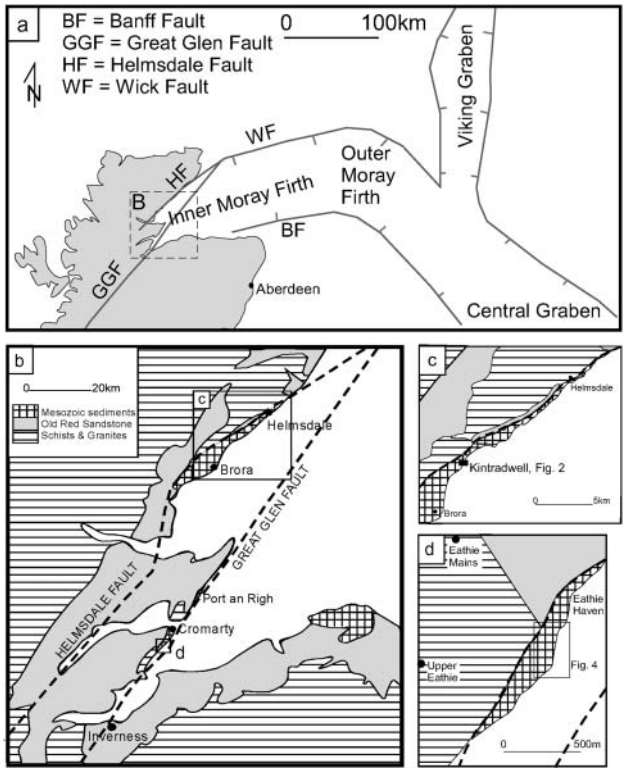

Fig. 1. (**a**) Regional setting of the Inner Moray Firth Basin within the western arm of the North Sea rift system. The dashed box indicates the location of (**b**). (**b**) Locations of the studied areas within the Jurassic outcrops of NE Scotland (modified after Bailey & Weir 1932). (**c**) Detail of the locality of the Kintradwell dyke. Location of map of Figure 2 is shown. (**d**) Detail of the locality of the sandstone injection complex at Eathie. Location of map of Figure 4 is shown.

is characterized by relative quiescence and thermal subsidence following late Jurassic rifting (Thomson & Underhill 1993).

The three study areas comprise sediments of Kimmeridgian age. Between Brora and Helmsdale the succession of boulder beds, carbonaceous siltstones, mudstones and sandstones has received considerable attention (Bailey & Weir 1932; Pickering 1984; Trewin & Hurst 1993). The Kintradwell sandstone dyke (Murchison, 1827) and the surrounding Kimmeridgian host rocks were studied in this area. The Kimmeridgian at Eathie is entirely developed in mudstone facies (Waterston 1951). Several limestone beds, up to about 0.5 m in thickness, occur within an otherwise uniform succession of black mudstones. The beds are penetrated by a complex of injected sandstones and minor faults (Waterston 1950). The exposure at Port an Righ comprises Kimmeridgian mudstones and limestones that are penetrated by numerous calcite-cemented fault planes.

Methods

Orientations of structures and their relation to the bounding faults (the Helmsdale Fault and the Great Glen Fault) were analysed to understand the kinematic relation between injected sandstones, fractures and faults. Palaeostress analysis was performed on orientations of dykes and slickensided fault planes. For palaeostress analysis the MS-DOS program tensor (Delvaux 1994) was used. Samples of cemented injected sandstones, cemented host sandstones and tectonic veins were selected from all three localities for diagenetic studies. All sections analysed microscopically were taken from the core of large samples (typically with dimensions of several tens of centimetres), well away from the weathering crust to avoid recent telodiagenetic effects. Samples with broken surfaces were first examined using SEM with a Link analytical AN10155S energy-dispersive system, after which samples were selected for polished thin-section manufacture. Cold cathodoluminescence (CL) microscopy was used to investigate the history of carbonate cementation in injected sandstones, host sandstones and carbonate-cemented fractures. Polished thin sections were examined using a Cambridge CITL Cold Cathodoluminescence 8200 mk3 system, with operating beam current conditions of 200–300 μA and an acceleration voltage of 15 kV. Hot CL microscopy was used to investigate quartz cements in sandstone injections. Polished thin sections were carbon coated and examined using an Oxford Instruments Limited Cathodoluminescence detector on a Link Analytical AN10155S electron-dispersive system. Operating beam current conditions were 30–70 μA with an acceleration voltage of 25 kV. On the same system, at beam current conditions between 3 and 5 nA, carbon-coated polished thin sections were used to determine the chemical composition of diagenetic minerals using a backscattered electron (BSE) detector. Samples for microthermometric analysis were prepared as doubly polished wafers and examined using a Linkam THM600 heating–freezing stage attached to a Nikon Optiphot2-POL microscope. For isotopic analysis of carbonate cements, samples of about 1 mg were drilled from polished slabs with a spatial resolution of about 1 mm. Sample powders were placed in a temperature-controlled block at 70 °C. Ultra-pure helium was used to purge all atmospheric gases. Samples were digested in 103% H_3PO_4 and were left for 8 h to react. Samples were transferred to the AP2003 Gas Prep Interface, where gas was extracted from the sample by overpressurizing with helium to 5 mbar. The gas switched through a small room-temperature gas chromatograph, which separated the CO_2 from any other traces of gas. The resulting gas was analysed using an AP2003 triple-collector mass spectrometer. The 1σ reproducibility of the system is ±0.1‰ for $\delta^{13}C$ and $\delta^{18}O$ values. All data are reported as per mil deviation from the V-PDB international standard.

Field data

Terminology

The definitions adopted here are that a sandstone sill is an intrusion concordant with bedding, and a sandstone dyke is an intrusion with a discordant relation to bedding. Terminology for geometric features of dykes and sills is taken from descriptions of igneous dykes and sills (Delaney *et al*. 1986). Dykes and sills are composed of segments that may overlap. Overlapping segments are either connected or unconnected. A composite sill or dyke refers to a setting where more than one overlapping segment occurs with the same general trend. A sill–dyke complex refers to several (composite) sandstone dykes and sills with varying orientations, in connection with each other.

The composite sandstone dyke at Kintradwell

The composite dyke at Kintradwell is exposed over a distance of *c*. 50 m and has a thickness ranging from about 0.2 to 1 m (Fig. 2). It was intruded into a succession of thinly bedded sandstones and carbonaceous silt and mudstones (Bailey & Weir 1932; Roberts 1989). The source for the sandstone dyke is not exposed. The composite dyke consists of two left-stepping, overlapping segments (Fig. 2). These segments trend *c*. 120°. Small-scale offshoots from the main dyke are observed that in 2D do not connect back into the main dyke (Fig. 3a). Well-cemented millimetre-thick bands occur within the dyke, that are absent within the host-rocks. These bands are oriented approximately parallel to the margins of the dyke (Fig. 3b). Their resistant character and anastomosing pattern suggest they are deformation bands (Aydin 1978; Mair *et al*. 2000). The dyke forms a ridge,

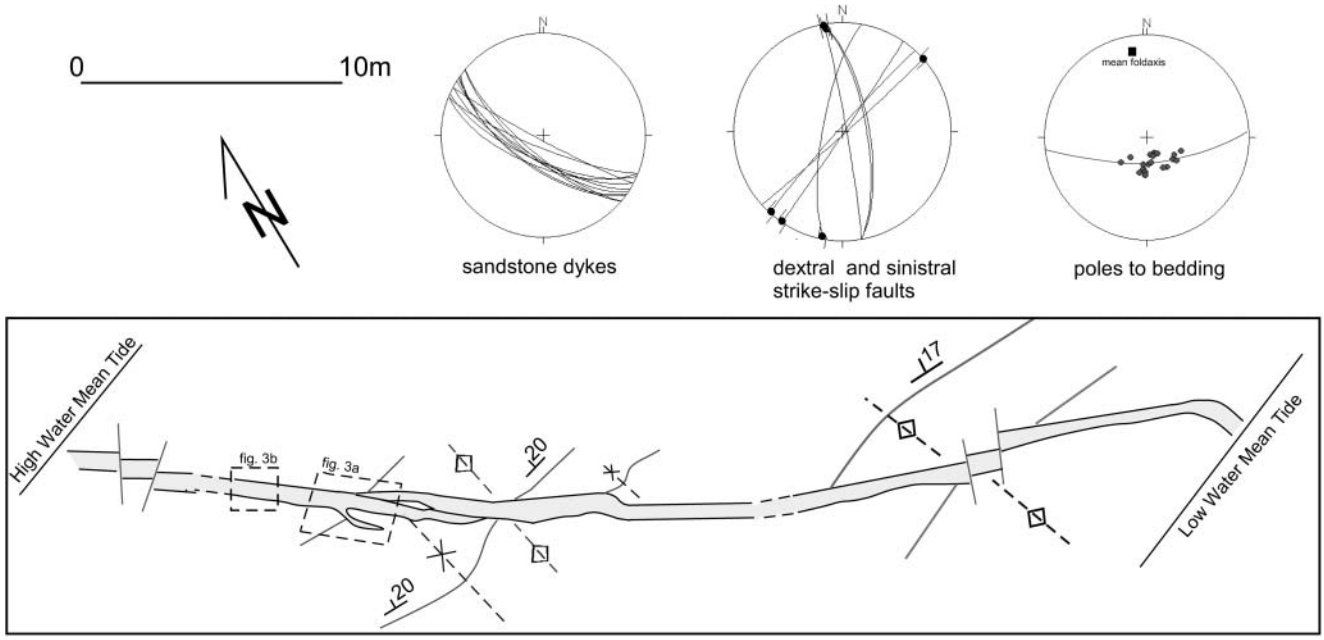

Fig. 2. Map of the composite dyke at Kintradwell, location shown in Figure 1. Width of the dyke has been exaggerated by a factor of two. Dyke is shown with grey shading. Dyke consists of two overlapping segments. Figure locations are indicated with dashed boxes. Stereonets show the orientations of several segments of the dyke, strike-slip faults that cut the dyke and poles to bedding, defining a north–south-trending fold-axis.

as a result of a pervasive calcite cement. Surrounding beds of host sandstone are also calcite cemented. Synsedimentary folds in the host rocks (Roberts 1989) have not deformed the dyke and fold axes can be traced across the dyke without shear movement, illustrating the pure opening mode of the composite dyke (Fig. 2). This also illustrates that dyke intrusion postdated soft sediment deformation. Later small-scale dextral and sinistral strike-slip faults cross-cut the dyke (Fig. 2).

The sandstone dyke–sill complex at Eathie

A sandstone dyke–sill complex was intruded into a sequence of black mudstones and decimetre-thick bands of limestone (Waterston 1950, 1951). The complex is exposed on a wave-cut platform and is composed of dykes and sills with thickness of 0.1–2 m penetrating at least 200 m of stratigraphy (Fig. 4). The host lithology was tilted post-intrusion. Bedding dips gently to the east near the low-water mark and becomes steeper, eventually vertical and overturned near the bounding fault at the high-water mark (Fig. 4). A large sill concordant with bedding is present within the vertically dipping host-rocks near the high-water mark. It is identified as a sill because of small discordant steps. The sill ranges in thickness between 0.1 and 2 m. Several dykes emanate from the sill into younger strata to the east. No dykes were found passing into older strata. Several kinks were found where dykes traverse into sills and back again (Fig. 5a). Overlapping left- and right-stepping,

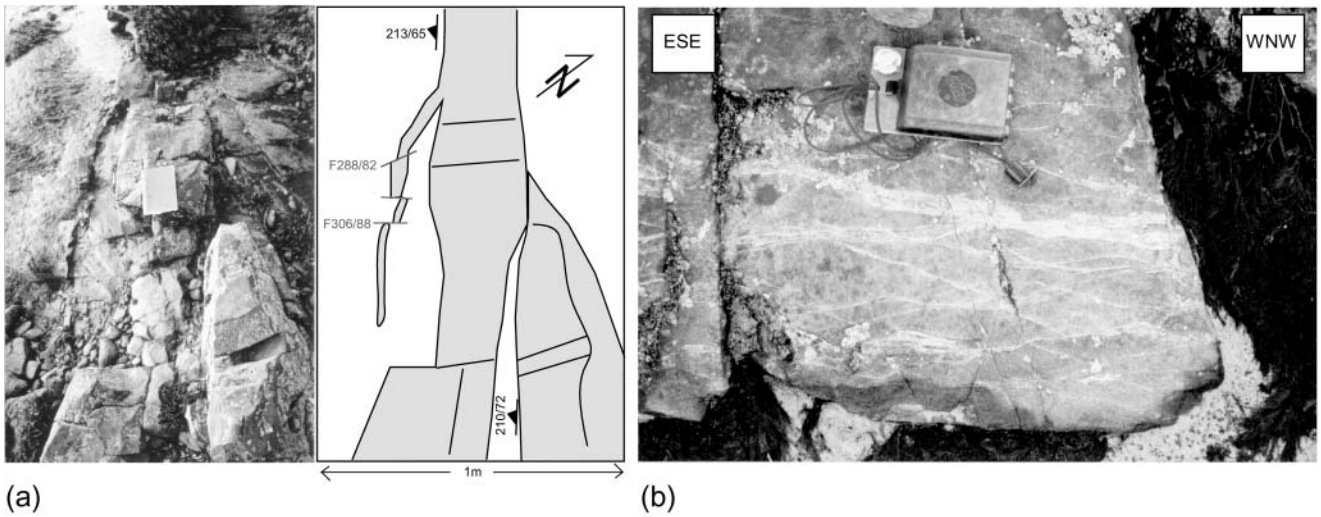

Fig. 3. (**a**) Photograph (left) and line-drawing (right) of small-scale offshoot along the composite dyke (shown with grey shading). Small-scale strike-slip faults offsetting the offshoot should be noted. Orientations of structures are indicated as dip-direction and dip. (**b**) Deformation bands within the Kintradwell dyke consist of white, anastomosing bands (sub)parallel to the dyke's margin.

pinch-out geometries were found (Fig. 5b). Bifurcation and thinning of dykes and sills are present both upwards and downwards in stratigraphy. Apart from post-intrusion tilting, strike-slip faults deform the dyke–sill complex (Fig. 4). Strike-slip faults both predate and postdate sandstone injections. The sandstone dyke–sill complex stands out because it is pervasively carbonate cemented. Well-cemented deformation bands are present within injected sandstones, trending subparallel to intrusion margins.

Calcite-cemented faults at Port an Righ

At Port an Righ (Fig. 1b), Kimmeridgian limestones and mudstones are separated from Devonian sandstones by a splay of the Great Glen Fault, trending 020°. Large numbers of calcite-cemented faults occur within the Kimmeridgian strata bounding the main faults. These faults are dominantly dextral strike-slip faults with NE–SW trends.

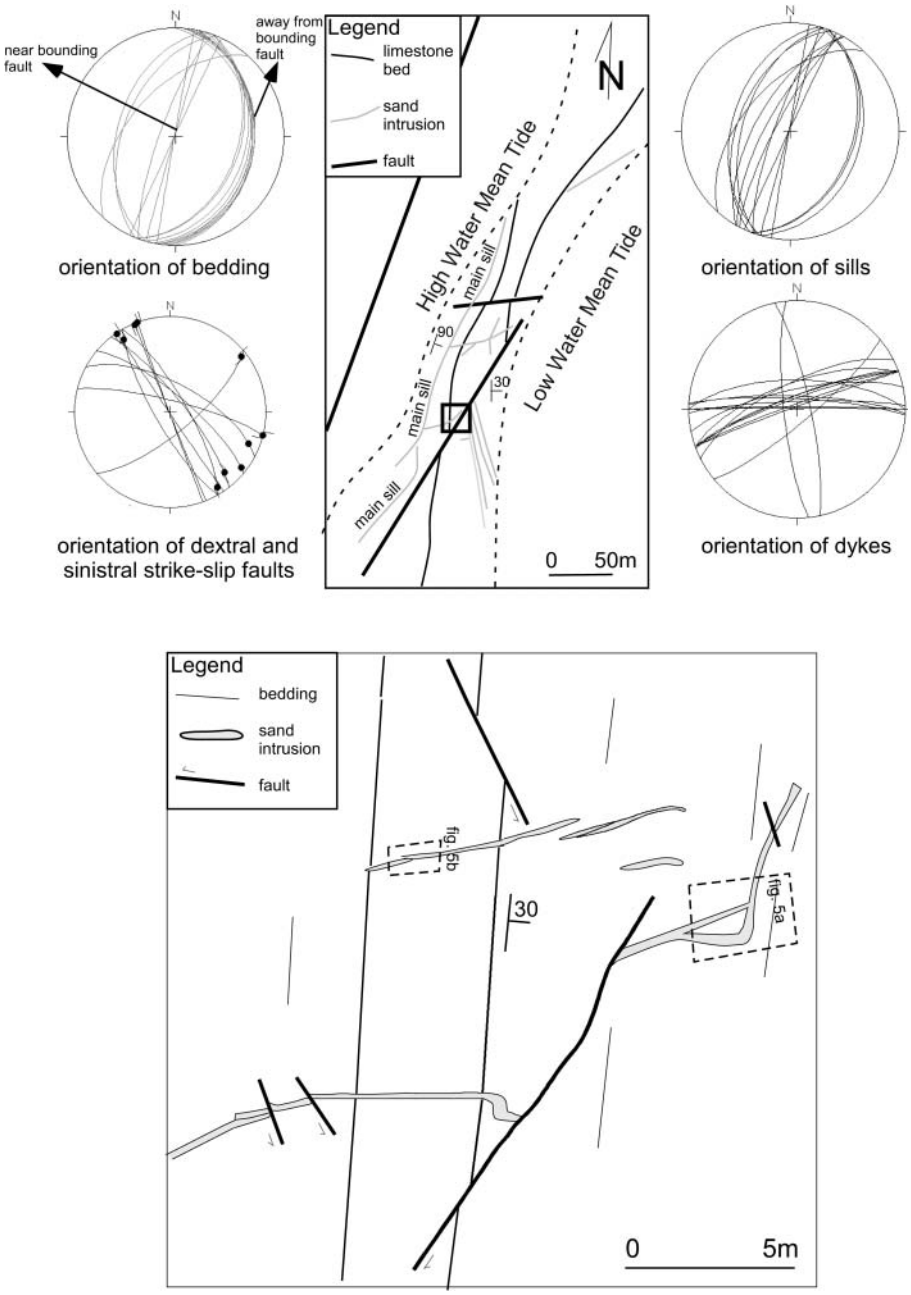

Fig. 4. Overview map of the outcrops at Eathie (upper map, location shown in Fig. 1d, modified after Waterston 1950) and a detailed map of some of the cross-cutting relations (lower map, location shown with square in upper map). Locations of Figure 5a and b are indicated with dashed boxes. Main trends and dips of bedding are indicated in both maps. Stereoplots show the main orientations of bedding, sills, dykes and slickensided fault planes.

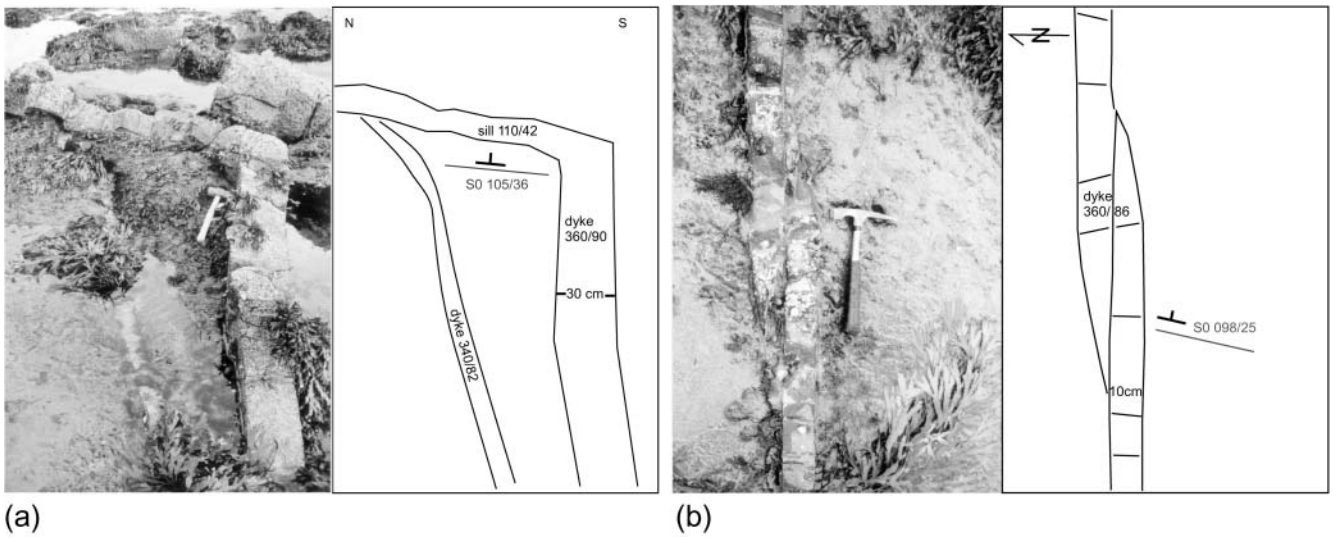

Fig. 5. (**a**) Kink, in which a dyke migrates into a sill into younger stratigraphy. The small-scale dyke shortcutting the kink should be noted. Orientations of structures are indicated as dip-direction and dip. (**b**) Composite dyke, made up of two overlapping dykes, each pinching out against the other. Orientations of structures are indicated as dip-direction and dip.

The diagenetic sequence

Injected sandstones

Dykes and sills are composed of *c*. 70% detrital grains and 30% fine-grained matrix and cements. The grains consist of 95% quartz and 5% K-feldspar and muscovite, are poorly to moderately sorted and range from 0.1 to 0.7 mm in size. Deformation bands are the oldest diagenetic imprint and have widths between 1 and 20 mm. Extreme grain-size reduction can be demonstrated (Fig. 6a). Brittle deformation is preserved as the occurrence of fractures within quartz grains that have been healed by authigenic quartz and by cataclastic flow of fragmented feldspar grains (Fig. 6a). The fact that quartz-filled fractures are abundant within deformation bands (Fig. 6a) but absent outside deformation bands (Fig. 6b) suggests that these fractures formed during the deformation process and were not inherited. Calcite is the main pore-filling cement. It also occurs as fracture-fills within grains (Fig. 7a). Calcite cement postdates deformation band development (Fig. 7b), is poikilotopic and partly replaces quartz at grain edges (Fig. 7c). The calcite cement within sandstone dykes and sills has an irregular zoned pattern composed of two luminescent cements (Fig. 7d). A dull orange–red luminescent calcite interlocks with a more dominant non-luminescent calcite. BSE imaging also reveals two types of calcite, a ferroan calcite interlocking with non-ferroan calcite (Fig. 7e). It is likely that the non-luminescent calcite corresponds to the phase that is ferroan, as iron is a quencher in carbonate luminescence (Marshall 1988). Apart from calcite cement, smaller amounts of fine-grained clay occur as pore-filling material. The clay is mainly illitic, which is thought to be authigenic because of its fibrous nature (Fig. 7f). It postdates calcite cement as the latest pore-filling material.

Host sandstones

Host sandstones at Kintradwell consist of *c*. 80% grains and 20% pore-filling matrix and cement. Grains consist of 90% quartz and 10% feldspar plus muscovite. Host sandstones are finer grained than the dykes that intrude them, with moderate sorting and grain-size range between about 0.03 and 0.3 mm (Fig. 8a). Sedimentary layering is manifested as alignment of grains and carbonaceous material (Fig. 8a). Calcite is the main pore-filling cement and replaces quartz grains at their edges. Calcite cement is poikilotopic and (Fig. 8b) fractured grains filled with calcite are rare. Cold CL shows all calcite is non-luminescent (Fig. 8c). BSE images confirm the uniform, ferroan nature of the calcite cement (Fig. 8d). Illite is the latest pore-filling mineral.

Tectonic veins

Tectonic veins occur at all localities and typically have widths ranging from 1 to 50 mm. All tectonic veins are composed of a single phase of bright luminescent calcite (Fig. 9a). The calcite commonly exhibits a beefy (fibrous) texture (Fig. 9b).

Comparing the diagenetic sequences

Figure 10 compares the diagenetic sequences within injected and host sandstones. Because of the similar luminescent and geochemical character, the non-luminescent ferroan calcite within sandstone injections is assumed to be the same as the non-luminescent ferroan calcite within the host sandstones. The relative age of the two types of calcite in injected sandstones cannot be determined from petrographic data. The diagenetic sequences for injected and host sandstones are broadly similar. There are, however, notable differences that will be examined in more detail using fluid inclusion and stable isotope data in the following section.

Diagenetic conditions during cementation

Fluid inclusion studies

Fluid inclusion petrography and fluid inclusion microthermometry (Goldstein & Reynolds 1994; Van den Kerkhof & Hein 2001) were performed to understand the origin and timing of quartz

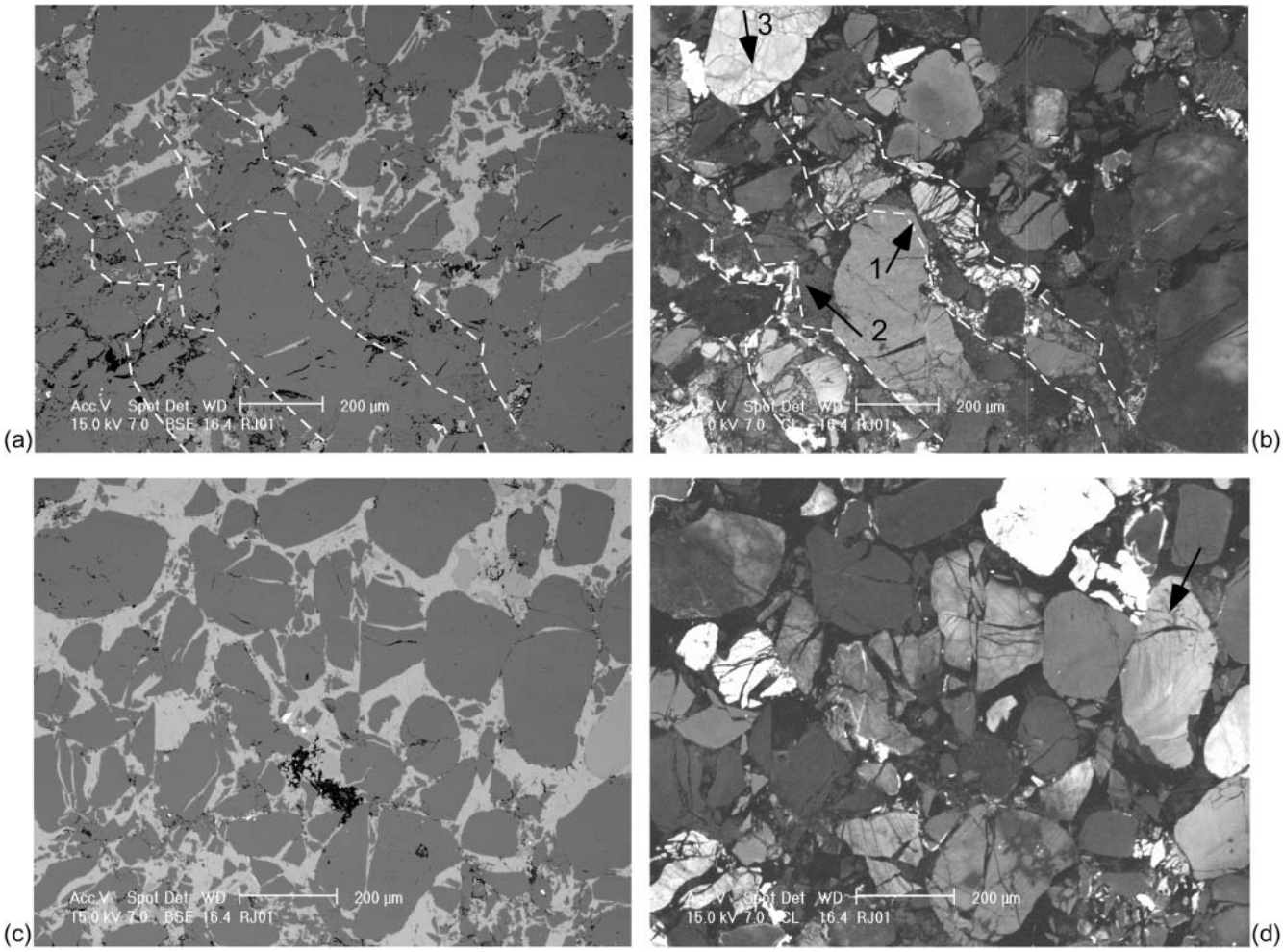

Fig. 6. BSE picture (**a**) and the same view under hot CL (**b**). Deformation bands can be clearly recognized (boundaries marked with white dashed lines) with extreme cataclastic deformation of grains. Fractured grains filled with authigenic quartz occur (arrow 1) alongside smeared-out zones of cataclastically deformed feldspar grains (arrow 2). Vague hairline fractures occurring within some clasts outside the deformation bands (arrow 3), which can be clearly separated from the vivid, thick authigenic fracture-fills within the deformation bands, should be noted. Kintradwell dyke. BSE picture (**c**) and the same view under hot CL (**d**) of a zone without deformation bands. One can clearly see that the clear fractures in the CL picture relate to calcite-filled fractures rather than quartz-filled fractures. Only vague hairline fractures can be detected, which are inherited (arrow). Kintradwell dyke.

and calcite cements within clastic intrusions as compared with the origin and timing of cements within host sandstones and tectonic veins (Table 1). All two-phase inclusions within quartz and calcite were examined by CL to determine the luminescent character of their host mineral following microthermometric measurements.

Fluid inclusion studies of injected sandstones. All analysed samples of injected sandstones display similar fluid inclusion assemblages (Tables 1 and 2). Two-phase secondary fluid inclusions occur as trails in quartz grains within deformation bands (Fig. 11a). Twenty-four measured fluid inclusions within trails could be confidently coupled to authigenic quartz fracture-fills when investigated under CL. The measured homogenization temperatures range from 78.3 to 111.9 °C (Table 2, Fig. 12a). Primary inclusions in calcite cement occur both as two-phase inclusions (scarce, Fig. 11b) and monophase inclusions (abundant). A total of 42 two-phase inclusions within carbonate cement were measured, with a 64.2–113.1 °C range in homogenization temperatures (Fig. 12a). Thirty-nine out of 42 measured inclusions could confidently be associated with the dull luminescent non-ferroan calcite. Final ice melting temperatures of two-phase inclusions show a considerable spread, translating to NaCl-weight-equivalent salinities (Fig. 12b) between 0 and 15% NaCl-weight-equivalent (Bodnar 1993). Colour changes marking the transformation from ice (solid) into water (liquid) were used to measure final ice melting temperature of monophase inclusions (Wilkinson *et al*. 1998). In nine cases this resulted in reproducible final ice melting temperatures, with salinities ranging from 1.9 to 4.6% NaCl-weight-equivalent (Fig. 13a).

Fluid inclusion studies of host sandstones. Only monophase inclusions occur within the two samples of host sandstones analysed from Kintradwell (Table 1). Sixteen reproducible final ice melting temperatures could be measured. Salinities calculated range from 1.5 to 7.0% NaCl-weight-equivalent (Fig. 13a).

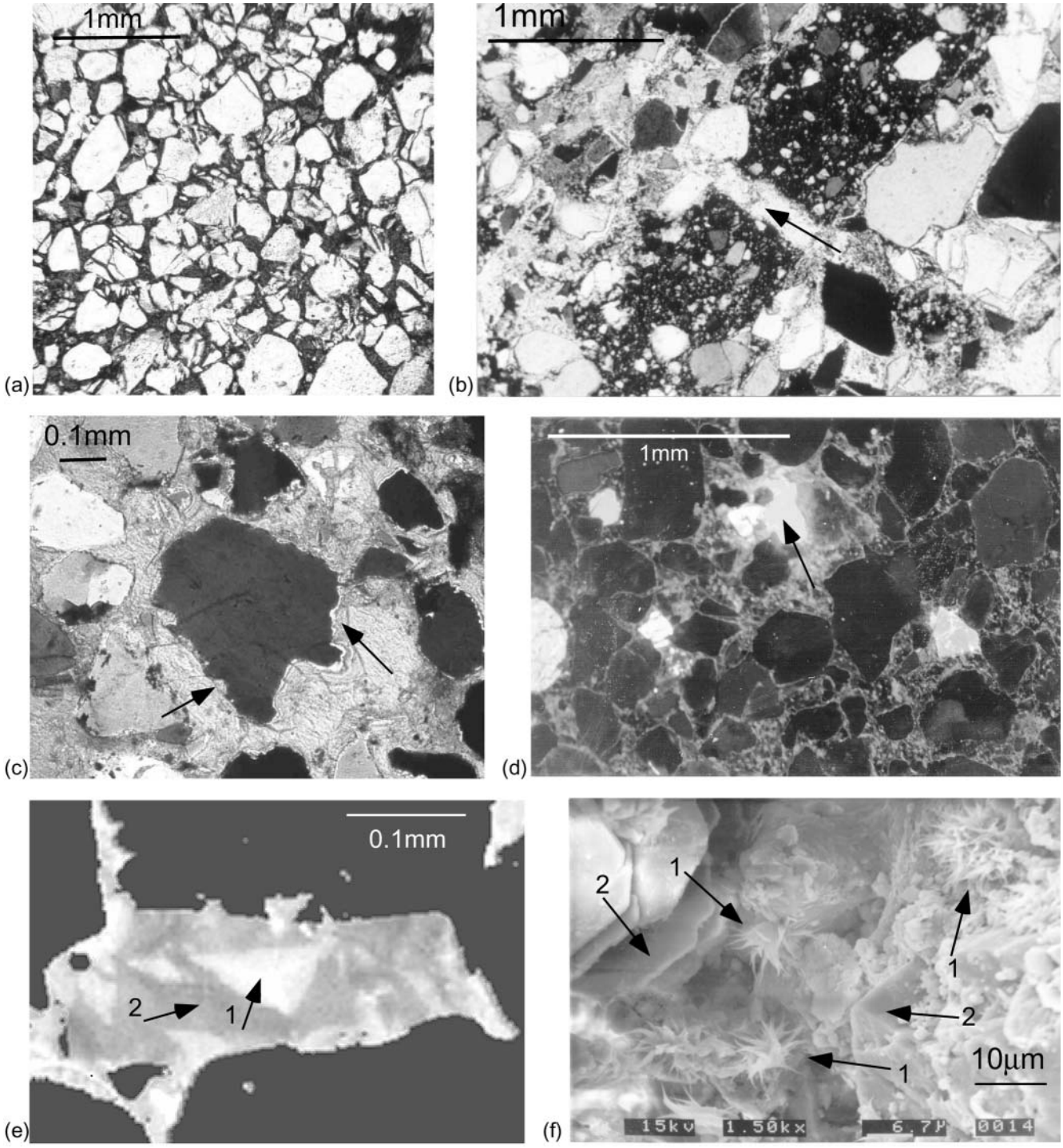

Fig. 7. (**a**) Micrograph showing stained thin section with calcite showing up in dark colours. Abundant fracture-filling calcite should be noted. Plane-polarized light. Kintradwell dyke. (**b**) Calcite cement fracturing an older deformation band (arrow). Pervasive fracturing of quartz grains by cement outside deformation band should be noted. Kintradwell dyke. (**c**) Micrograph showing detail of dissolution of quartz grains by calcite (arrows). Crossed polars. Sill at Eathie. (**d**) Cold CL image of sandstone dykes shows an interlocking pattern of dull luminescent calcite and non-luminescent calcite. The occurrence of a limestone fragment (arrow) should be noted. Feldspar grains are bright grey, quartz grains are black. Kintradwell dyke. (**e**) BSE image of sandstone dyke showing two interlocking calcites, a brighter slightly ferroan calcite (arrow 1) and a non-ferroan calcite (arrow 2). Quartz grains are black. Kintradwell dyke. (**f**) Fibrous illite (arrows 1) overgrows earlier pore-filling calcite cement (arrows 2). Kintradwell dyke.

Fluid inclusion studies of calcite veins. Two-phase inclusions occurring within two sampled calcite veins show a range (62.1–108.3 °C) of homogenization temperatures similar to that for two-phase inclusions occurring within injected sandstones (Fig. 13b). Final ice melting temperatures translate into NaCl-weight-equivalent salinities between 2 and 8% (Fig. 13c).

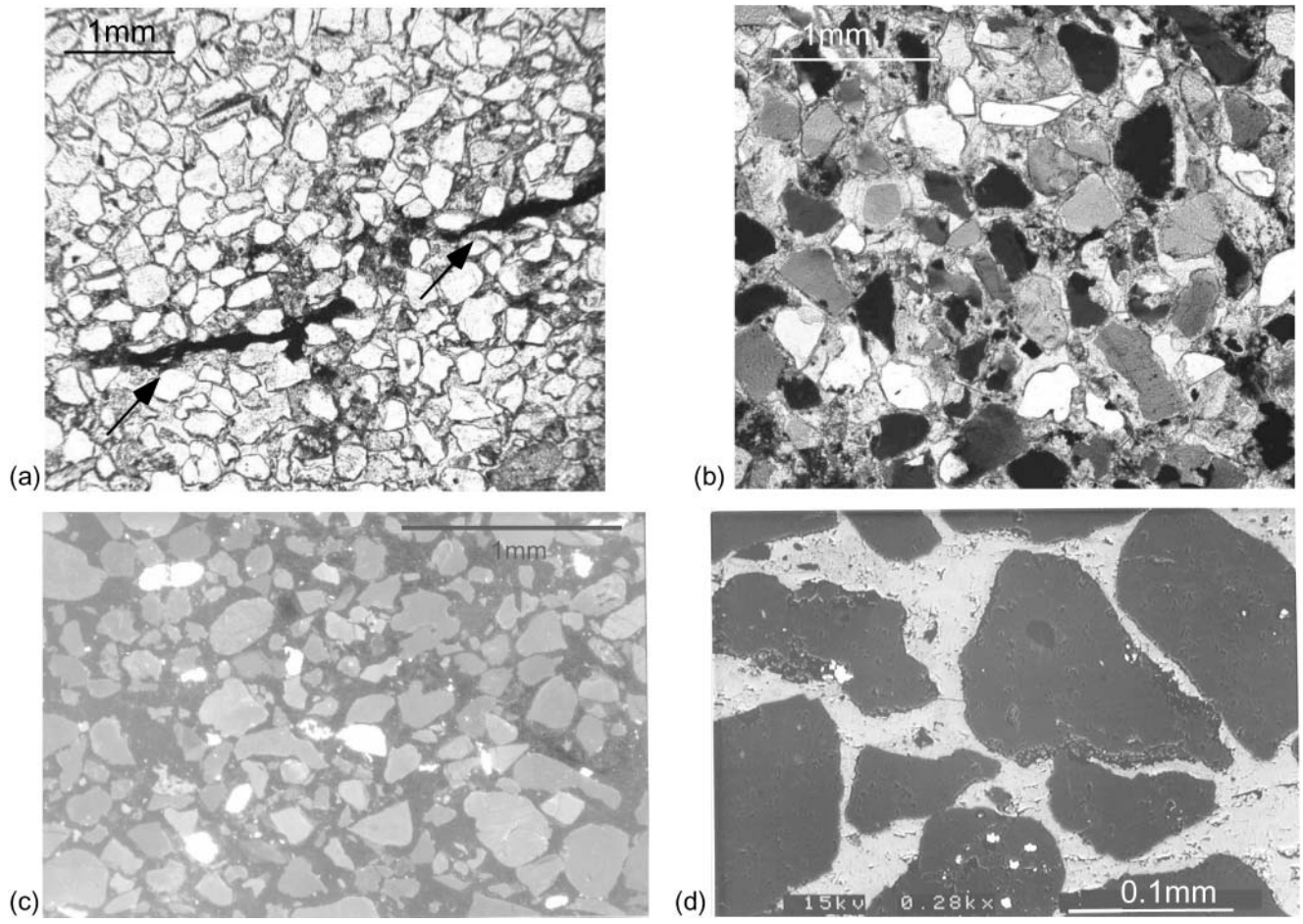

Fig. 8. (**a**) Micrograph showing general appearance of the host sandstones. Layers of carbonaceous material (arrows) should be noted. Plane-polarized light. Host sandstone at Kintradwell. (**b**) Micrograph showing character of calcite cement within host sandstones. Crossed polars. Host sandstone at Kintradwell. (**c**) Micrograph taken with cold CL. Host sandstones show only non-luminescent calcite. Host sandstone at Kintradwell. (**d**) BSE image of host sandstone showing uniform ferroan calcite cement. Host sandstone at Kintradwell.

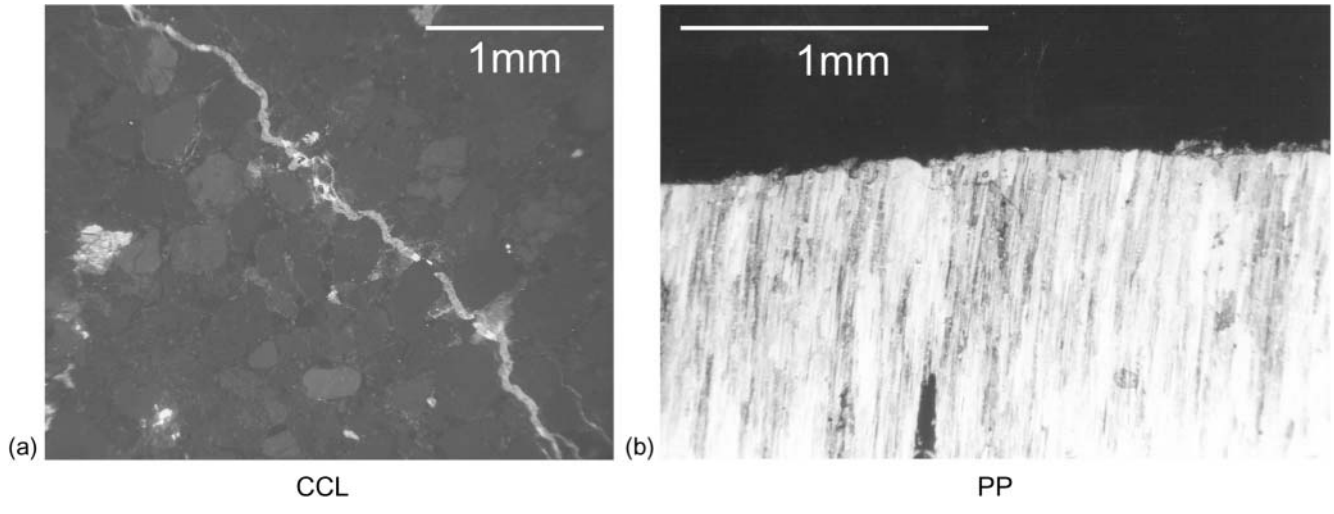

Fig. 9. (**a**) Fractures filled with bright luminescent calcite are the latest phase of carbonate cementation. Fractures can have widths up to several centimetres. This vein cuts through a dyke at Eathie. (**b**) Micrograph illustrating the fibrous nature of calcite veins. Plane-polarized light. Vein from Port an Righ cutting through lime mudstone.

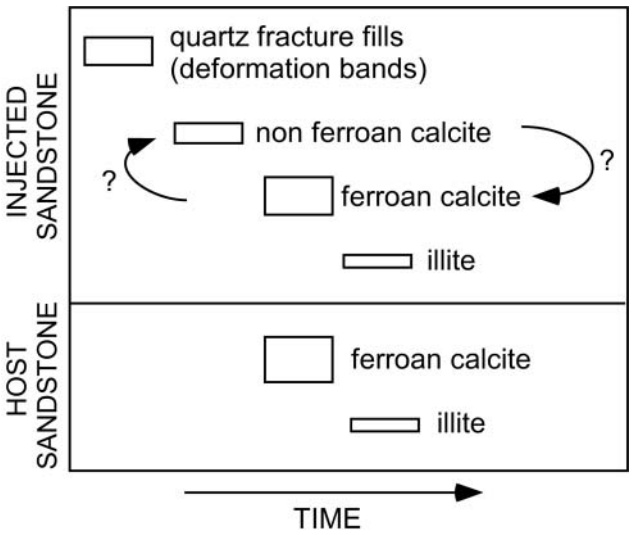

Fig. 10. General diagenetic sequences of injected sandstones compared with host sandstones. Thickness of box is an indication of the relative importance of each diagenetic event.

C/O Stable isotopes

C/O stable isotope ratios were measured for bulk carbonate cements within various hosts. The resolution of sampling does not allow the different luminescent calcite cements to be separated. The isotopic composition of calcite in various hosts does not vary greatly (Fig. 14). Carbon isotope values ($\delta^{13}C$) for calcite cement in sandstones and veins range from +0.77 to −3.4‰, whereas oxygen isotope values ($\delta^{18}O$) for the same suite range from −7.99 to −12.19‰. Although the whole group clusters well, there are some notable differences between the subgroups. The signatures in host sandstones cluster around 0‰ for $\delta^{13}C$, whereas the signatures within the calcite in sandstone injections and within tectonic veins occurring near the sandstone injections show slightly more depleted $\delta^{13}C$ values, −3‰. Calcite-filled veins at Port an Righ show the strongest depletion in $\delta^{18}O$ values (−12‰), whereas the calcite cement in host sandstones shows the least depleted $\delta^{18}O$ values −8 to −9‰. Calcite cements in sandstone injections have $\delta^{18}O$ values around −9 to −10‰.

Discussion

Geometric relations between sandstone dykes and faults

Figure 15 shows palaeostress analyses (Delvaux 1994) performed on sandstone dykes and striated fault planes encountered in the three exposures. If we assume that sandstone dykes are opening mode (hydraulic) fractures (Cosgrove 2001), the orientations of the three principal stress axes during dyke intrusion can be deduced (Fig. 15a). Figure 15b shows a palaeostress analysis of striated fault planes encountered in the three analysed exposures. The similarity between the deduced orientations of principal stresses in both diagrams suggests that both sand injections and faulting took place within the same stress regime. The observation of injected sandstones cross-cutting and being cut by cemented fault planes suggests that both events were more or less coeval. Within this stress regime, the bounding Helmsdale and Great Glen faults would act as dextral strike-slip faults, which has important consequences for the timing of sand injec-

Table 1. *Summary of fluid inclusion petrography of the analysed samples*

Sample	Host	Contents at room temperature	Occurrence	Size range (μm)	Morphology	Degree of fill (liquid to vapour ratio)	Comments
Kintradwell dyke	Quartz	L_1V_1	S; intragranular planes	3–5	Equant to elongate	0.8–0.9	Abundant in deformation bands
	Calcite	L_1V_1	P; isolated	1–5	Prismatic	0.95	Scarce throughout
	Calcite	L	P; isolated	1–3	Prismatic	1.00	Moderately occurring
Eathie sill	Quartz	L_1V_1	S; intragranular planes	3–7	Equant to elongate	0.7–0.9	Abundant in deformation bands
	Calcite	L_1V_1	P; isolated	1–4	Prismatic to elongate	0.92–0.95	Scarce throughout
	Calcite	L	P; isolated	1–3	Prismatic	1.00	Moderately occurring
Eathie dyke	Calcite	L_1V_1	P; isolated	1–5	Prismatic to elongate	0.94–0.95	Scarce throughout
	Calcite	L	P; isolated	1–3	Prismatic	1.00	Moderately occurring
Kintradwell host sandstone adjacent to dyke	Calcite	L	P; isolated	1–4	Prismatic to elongate	1.00	Moderately occurring
Kintradwell host sandstone 50 m from dyke	Calcite	L	P; isolated	1–4	Prismatic to elongate	1.00	Moderately occurring
Calcite vein, Kintradwell	Calcite	L_1V_1	P; isolated	1–5	Prismatic to elongate	0.95	Scarce throughout
	Calcite	L	P; isolated	1–3	Prismatic	1.00	Moderately occurring
Calcite vein, Eathie	Calcite	L_1V_1	P; isolated	1–6	Prismatic to elongate	0.94–0.96	Scarce throughout
Calcite vein, Port an Righ	Calcite	L_1V_1	P; isolated	1–6	Prismatic to elongate	0.94–0.97	Scarce throughout

L, liquid; V, vapour; P, primary; S, secondary.

Table 2. *Summary of fluid inclusion microthermometry*

Sample	Host	Occurrence	System	T_e range	T_m range (mean)	T_h range (mean)
Kintradwell dyke	Quartz	Secondary	H_2O–NaCl–$MgCl_2$	−40 to −21	n.d.	78.3–88.9 (83.7)
	Calcite	Primary	H_2O–NaCl–$MgCl_2$	−37 to −22	−12.7 to −0.1 (−5.9)	68.3–94.2 (74.6)
Eathie sill	Quartz	Secondary		n.d.	n.d.	82.2–111.9 (98.2)
	Calcite	Primary	H_2O–NaCl–KCl	−30 to −25	−9.8 to −3.2 (−7.1)	64.2–108.7 (80.2)
Eathie dyke	Calcite	Primary	H_2O–NaCl–KCl	−25 to −22	−8.0 to −0.4 (−5.1)	65.7–113.1 (97.5)
Calcite vein, Eathie	Calcite	Primary		n.d.	−5.1 to −2.3 (−4.0)	68.1–85.2 (76.2)
Calcite vein, Port an Righ	Calcite	Primary	H_2O–NaCl	−17 to −15	−4.2 to −1.3 (−3.1)	62.1–108.3 (78.0)

T_e, eutectic temperature; T_m, final ice melting temperature; T_h, homogenization temperature; n.d., not determined.

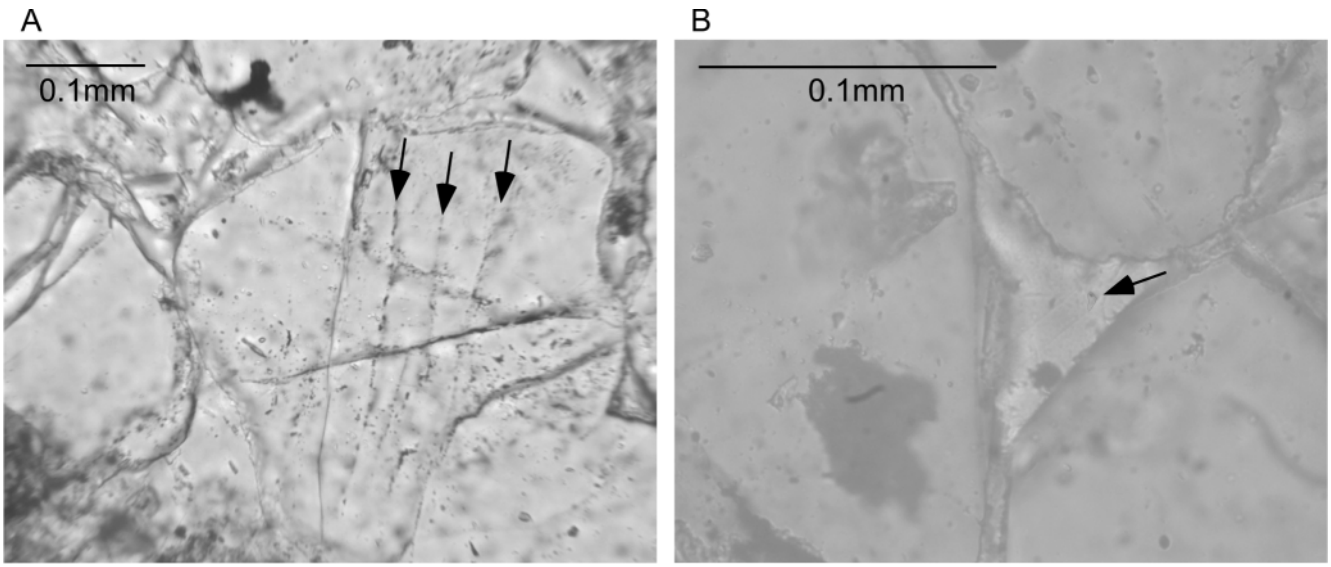

Fig. 11. (**a**) Example of secondary trails of fluid inclusions (arrows) within quartz grain within deformation band. Kintradwell dyke. (**b**) Example of two-phase fluid inclusion (arrow) within calcite cement. Eathie dyke.

tion. The late Jurassic was mainly characterized by dip-slip faulting along the Great Glen and Helmsdale faults (Thomson & Underhill 1993) and the subsequent early Cretaceous was a period of relative quiescence. Fracturing and sand injection related to dextral strike-slip deformation along the bounding faults could have occurred as late as the Tertiary, provided the source sand remain unlithified.

The origin of deformation bands in sandstone dykes and sills

The deformation bands found in sandstone dykes and sills are true cataclastic deformation bands (*sensu* Aydin 1978). Deformation bands occur within injected sandstones and do not occur within host-sandstones, which suggests that deformation band development was related to a process taking place exclusively within injected sandstones. Deformation bands with fracture-filling quartz are the earliest diagenetic imprint, and they formed soon after the intrusion process. We believe that these deformation bands originated in the latest phase of injection, when fluids moved out of the injection structures and grains became in contact with one another. Sandstone dykes and sills would have greater initial width during their fluidized state. After fluidization ceased and the fluid pressure dropped, walls contracted, resulting in increased grain contact stresses, and bands parallel to the margins developed. Authigenic fracture-filling quartz was internally derived from solution at grain–grain contacts within deformation bands and reprecipitated at fresh, fractured grain surfaces (Fisher *et al*. 2000).

The origin of calcite cement types

A comparison between all the techniques used to analyse calcite cements reveals subtle differences between injected and depositional sandstones. The co-occurrence of a fluid inclusion assemblage consisting of monophase (all liquid) and moderately consistent two-phase inclusions can be interpreted as one assemblage formed below about 50 °C that was partially re-equilibrated (Goldstein 2001). The primary nature of the fluid inclusions within calcite is not easily proved, as neither negative crystal shapes nor fluid inclusion planes along growth zones within the calcite were observed (Roedder 1984). However, the consistent occurrence of this fluid inclusion assemblage within sandstone injections compared with the consistent occurrence of monophase (all liquid) inclusion within host sandstones suggests that two genuine populations of fluid inclusions occur within sandstone injections. Furthermore, two-phase fluid inclusions have consistent liquid–vapour ratios (Table 1), suggesting they have not stretched and leaked.

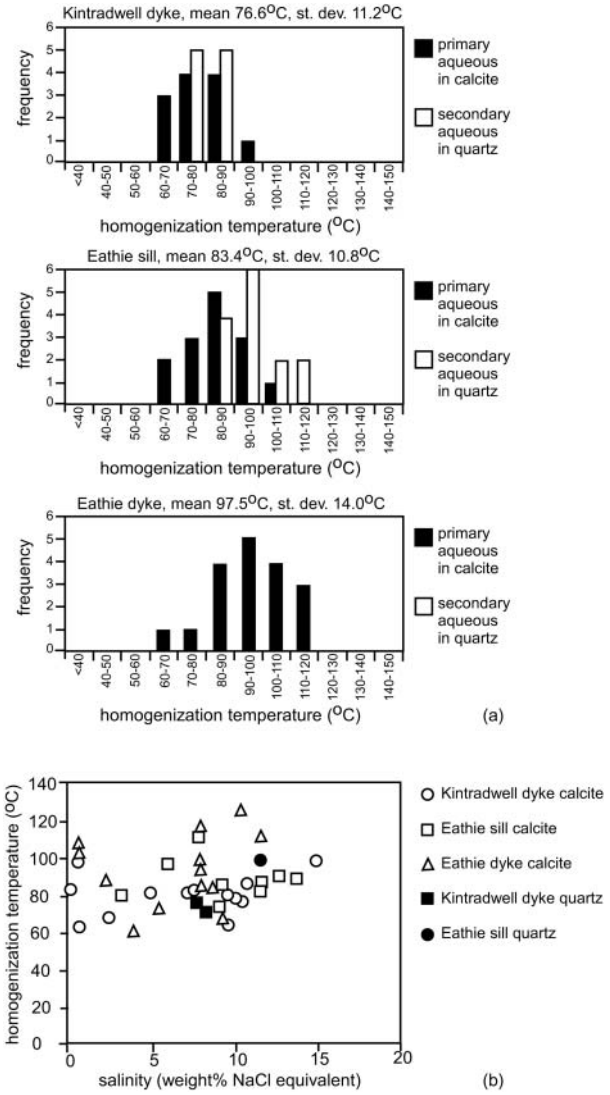

Fig. 12. (**a**) Fluid inclusion histograms of three sandstone injections, showing homogenization temperatures v. frequency of two-phase aqueous inclusions. (**b**) Salinity v. homogenization temperatures of two-phase fluid inclusions measured in sand injections. Total of 41 measurements.

Non-luminescent ferroan calcite. This type of cement makes up about 70% of the carbonate within injected sandstones and the total of cement within host sandstones. Ferroan calcite contains monophase inclusions, suggesting trapping below 50 °C (Goldstein 2001). Final ice melting temperatures and $\delta^{13}C$ values for calcite cement in host sandstones suggest sourcing from marine bicarbonate (Macaulay *et al*. 1992, 2000; Goldstein 2001). Using the fractionation equation for calcite of Friedman & O'Neil (1977) and assuming an initial marine pore fluid with $\delta^{18}O$ of −1‰ SMOW (on average the composition of sea water; Shackleton & Kennett 1975; Watson *et al*. 1995) precipitation temperatures close to 50 °C are calculated (Fig. 16). This temperature is consistent with the observation of monophase inclusions within these cements. Thus this calcite precipitated from sea water at temperatures close to 50°C. A late (post-compaction) timing for the precipitation of this calcite is inferred by the relatively low minus-cement porosities (around 20%) observed within the depositional sandstones.

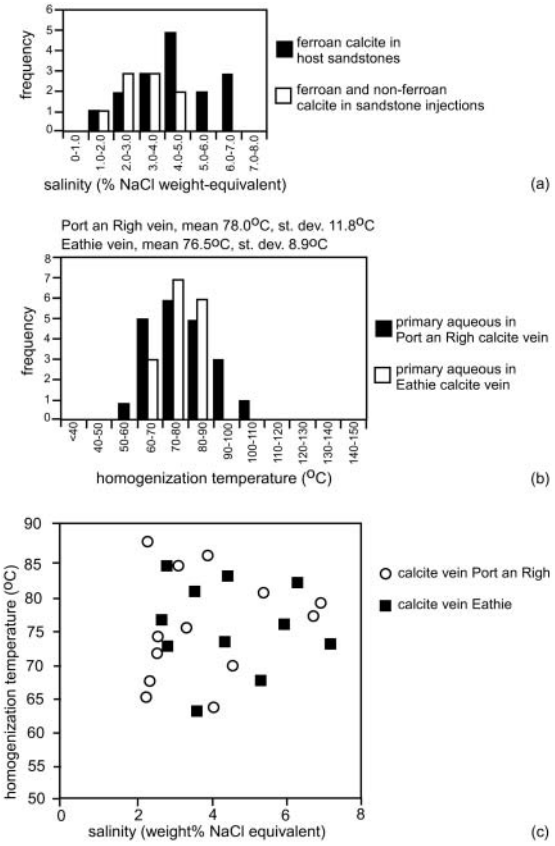

Fig. 13. (**a**) Salinity histogram for monophase, all liquid aqueous inclusions occurring in both sandstone injections and in host sandstones. (**b**) Fluid inclusion histogram showing homogenization temperature v. frequency for two analysed calcite-filled veins. (**c**) Salinity v. homogenization temperature of two-phase inclusions measured in calcite-filled veins.

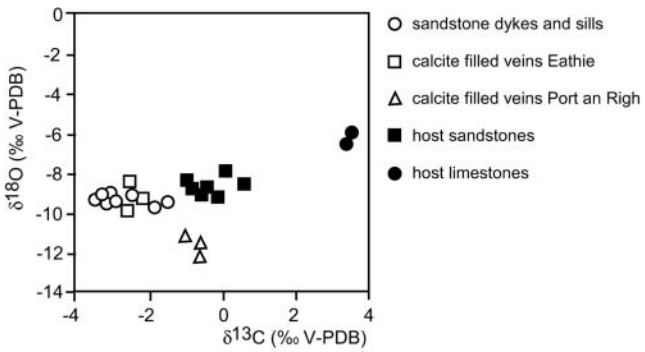

Fig. 14. C/O stable isotope results of all analysed calcite cements.

Luminescent calcite. This type of calcite makes up the bulk of the calcite veins and forms about 30% of the carbonate cement within sand injections. It contains two-phase fluid inclusions with considerable spread in homogenization and final ice melting temperatures. Using the mean homogenization temperature of about 78 °C for calcite veins (Fig. 13b) together with the mean $\delta^{18}O$ of −12‰ for calcite veins, the original $\delta^{18}O$ of the fluid from which this high-temperature calcite precipitated would be around −2‰ to −3‰ SMOW (Fig. 16), although there is considerable uncertainty in the actual composition, as a result of

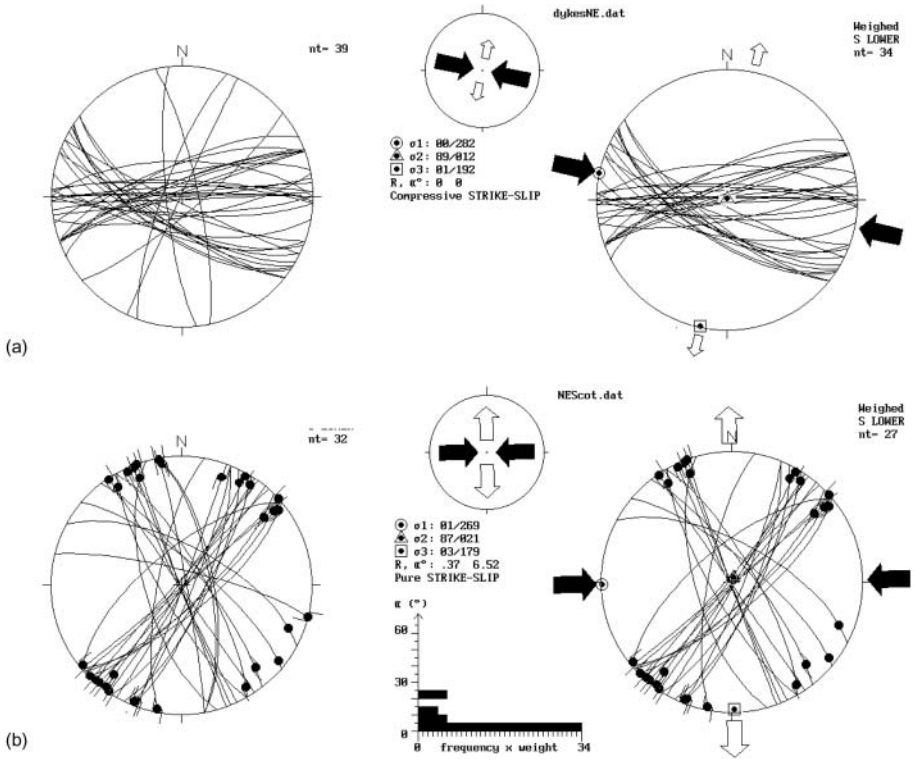

Fig. 15. (**a**) All measured sandstone dykes (left) and the best fit stress tensor (right) fitting 34 out of 39 measurements. All data have been corrected for post-intrusion tilting. (**b**) All measured slickensided faultplanes (left) and the best fit stress tensor (right) fitting 27 out of 32 measurements. Frequency histogram shows the deviation α between the striation direction measured and the theoretically calculated striation direction fitting the tensor. All data have been corrected for post-intrusion tilting.

the large range of homogenization temperatures measured. The $\delta^{18}O$ value of calcite cement in sandstone injections is a mixture of the two types of calcite. The mean value of −9.5‰ is consistent with a mixture of about 70% of the non-luminescent ferroan type, which precipitated at about 50 °C and about 30% of the non-ferroan, dull luminescent type, which precipitated at temperatures between 70 and 100 °C (Fig. 16). These ratios are in accordance with the observations made with CL (Fig. 7d). The shift towards lower $\delta^{13}C$ values of calcite in the sandstone dykes and sills suggests that the non-ferroan, dull luminescent type has a $\delta^{13}C$ of about −8‰ (to have the mixed signature of about −2‰). This suggests that some of the carbon for this type of calcite is derived from organic matter (Macaulay *et al*. 1992), which is abundant within mudstone clasts in injected sandstones. Organic maturation (Cheser & Bacon 1975; Pearson & Watkins 1983; Hillier & Marshall 1992) and clay mineralogy (Hurst 1982) of Upper Jurassic sediments in the Inner Moray Firth Basin indicates a thermal maximum of 50–60 °C for the Brora–Helmsdale area. This implies that the two-phase fluid inclusion temperatures from sand injections are anomalously high in the context of their host strata. There are no nearby igneous intrusions of Jurassic to recent age that could have caused a very local heat-source for this anomaly. We suggest that the fluid from which this type of calcite precipitated originated from deeper (hotter) strata and was brought up with sufficient velocity to maintain an anomalous temperature. The exact depth from which this fluid originated cannot be estimated (the depth depending on the velocity at which the fluid travelled upwards and the rate of cooling the fluid experienced). The large range of homogenization temperatures of fluid inclusions, the considerable spread in salinities and the coexistence of monophase and two-phase fluid inclusions within this type of calcite suggest that the hot, more saline basinal fluid mixed with the cool, marine pore fluid present within the host to give a large range of temperatures and compositions.

The relative timing of the two carbonate cements. The exclusive occurrence of a high-temperature calcite within sandstone injections and calcite veins suggests that the origin of this calcite is linked to an event taking place only within injections and fractures. Broadly similar fluid inclusion data from quartz fracture-fills in deformation bands and from the high-temperature calcite suggest that both precipitated early in the presence of the relatively hot, saline fluid phase. Because deformation band development predates large-scale carbonate precipitation, this relatively hot, saline fluid precipitated the first phase of calcite. A younger phase of calcite, precipitating at temperatures close to 50 °C, completely cemented both host sandstones and sandstone injections. The fluids responsible for the early phase of carbonate precipitation in injected sandstones came from a deeper-seated saline brine that was brought rapidly upward into Kimmeridgian strata (before too much cooling). There are many ways to exceed the supersaturation of $CaCO_3$ and cause calcite precipitation (Zhang & Dawe 1998). One factor that may control early calcite precipitation in sand injections is pressure drops that occurred shortly after fluidization ceased. If the pressure decreases, dissolved CO_2 can be released from solution, causing the solution pH to rise (Zhang & Dawe 1998). Consequently, the water can become supersaturated with $CaCO_3$, causing calcite precipitation, even though the fluid might be cooling at the same time (Fisher & Boles 1987; Morad 1998; Zhang & Dawe 1998). A later phase of relatively cold fluids (<50 °C), probably percolating sea water, was responsible for precipitating calcite with $\delta^{13}C$ around 0‰ in both injected and depositional sandstones. The low minus-cement porosities (around 20%) observed within host sandstones support a late (post-compaction) origin for this calcite.

Timing and origin of injection

A direct relation between the injected sandstones and a source

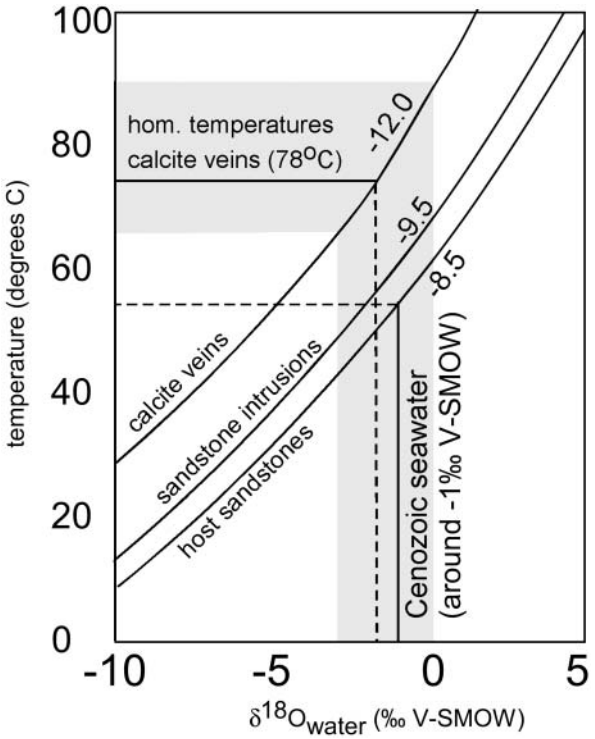

Fig. 16. Range of temperature and isotopic composition of the pore fluids constrained from the isotopic and fluid inclusion analysis of calcite cements (fractionation equation for calcite after Friedman & O'Neil 1977). The grey area indicates the error range for determining the pore-fluid composition from fluid inclusion data of tectonic veins (the error used being the range of standard deviations from the means determined in Fig. 14b).

sandstone cannot be seen in any of the outcrops. At Eathie and Port an Righ, no sandstones are exposed within the Jurassic section. The host sandstones at Kintradwell do not qualify as a potential source, given their very fine-grained character (grain-size up to 0.3 mm) compared with the sandstone injections (grain-size up to 0.7 mm). The best candidate for the source is underlying Oxfordian sandstones, exposed south of the Kintradwell dyke. They have a coarser grain-size than the Kimmeridgian sands that would fit better with the grain-size distribution within the sandstone injections. The anomalously high temperature of the fluid from which the early diagenetic calcite and quartz precipitated provides another line of evidence suggesting upward injection. Deeper-seated, saline basinal fluids migrated upward along the bounding Great Glen and Helmsdale faults in response to dextral strike-slip movements (earthquakes). Fluids escaping along the bounding faults at shallow levels fluidized uncemented Oxfordian sands, which were subsequently injected into the overlying Kimmeridgian strata. From the coincidence between the palaeostress orientations deduced from both sand dykes and fractures (Fig. 15) it appears that the trigger for sand injection was dextral strike-slip movement along the Great Glen and Helmsdale faults. Thomson & Underhill (1993) found no evidence for dextral strike-slip on the Great Glen Fault during the Late Jurassic. If dextral strike-slip movement on the Great Glen Fault was the trigger for the release of hot brines from depth it may be that sand injection took place during Tertiary strike-slip movement (Thomson & Underhill 1993; Underhill & Brodie 1993). A late timing of sand injection is also supported by the sharp nature of intrusion margins and the absence of differential compaction features, suggesting that the Kimmeridgian sequence of mudstones, siltstones and fine-grained sandstones had undergone sufficient compaction to be deformed in a brittle manner.

Conclusions

Sand injection within Kimmeridgian strata sourced from underlying Oxfordian sands took place when basinal fluids moved upward along the basin-bounding Helmsdale and Great Glen faults in response to dextral strike-slip motion, probably during the Tertiary. The basinal fluid had anomalous temperatures (homogenization temperatures between 70 and 100 °C) compared with the recorded thermal maturation of the host Kimmeridgian strata (50–60 °C). This suggests that these fluids were brought up along bounding faults and fractures with sufficient velocity to retain an anomalous temperature. The spread in homogenization temperatures and salinities measured is due to mixing of the hot, saline fluid driving injection with the relatively cool, lower-salinity pore fluids present within the host sediments. Deformation bands and early calcite cement develop upon wall-rock contraction after fluidization ceased and fluid pressures dropped. Upon burial, both depositional and injected sandstones were further cemented with ferroan calcite at temperatures close to 50 °C.

G. Watt and N. Bordas-Lefloch are thanked for assistance with SEM–CL and fluid inclusion microthermometry, respectively. K. Bjørlykke is thanked for reviewing an earlier version of this manuscript. Journal reviewers D. Dewhurst, J. Macquaker and R. Worden significantly improved the quality of the manuscript. The members of the Injected Sands Consortium (ChevronTexaco, Shell, Norsk Hydro, KerrMcGee, Statoil and TotalFinaElf) are thanked for financial support.

References

Aydin, A. 1978. Small faults formed as deformation bands in sandstone. *Pure and Applied Geophysics*, **116**, 913–930.

Bailey, E.B. & Weir, J. 1932. Submarine faulting in Kimmeridgian times: east Sutherland. *Transactions of the Royal Society of Edinburgh*, **57**, 429–467.

Barr, D. 1985. 3D palinspastic restoration of normal faults in the Inner Moray Firth: implications for extensional basin development. *Earth and Planetary Science Letters*, **75**, 191–203.

Bird, J.T., Bell, A., Gibbs, A.D. & Nicholson, J. 1987. Aspects of strike-slip tectonics in the Inner Moray Firth Basin, offshore Scotland. *Norsk Geologisk Tidsskrift*, **67**, 353–369.

Bodnar, R.J. 1993. Revised equation and table for determining the freezing point depression of H_2O–NaCl solutions. *Geochimica et Cosmochimica Acta*, **57**, 683–684.

Cheser, J.A. & Bacon, M. 1975. A Deep Seismic Survey in the Moray Firth. Institute of Geological Sciences Report, **75/11**, 1–13.

Cosgrove, J.W. 2001. Hydraulic fracturing during the formation and deformation of a basin: a factor in the dewatering of low-permeability sediments. *AAPG Bulletin*, **85**(4), 737–748.

Delaney, P.T., Pollard, D.D., Ziony, J.I. & McKee, E.H. 1986. Field relations between dikes and joints: emplacement processes and palaeostress analysis. *Journal of Geophysical Research*, **91**, 4920–4938.

Delvaux, D. 1994. *Tensor interactive MS-DOS Quick Basic program developed for palaeostress determinations on geological fractures and earthquake focal mechanisms. Version 2.9*. Royal Museum for Central Africa, Tervuren.

Diller, J.S. 1890. Sandstone dikes. *Geological Society of America Bulletin*, **1**, 411–442.

Dixon, R.J., Schofield, K., Anderton, R., Reynolds, A.D., Alexander, R.W.S., Williams, M.C. & Davies, K.G. 1995. Sandstone diapirism and clastic intrusion in the Tertiary Submarine fans of the Bruce–Beryl Embayment, Quadrant 9, UKCS. *In:* Hartley, A.J. & Prosser, D.J. (eds) *Characterization of Deep Marine Clastic Systems*. Geological Society, London, Special Publications, **94**, 77–94.

Donato, J.A. & Tully, M.C. 1981. A regional interpretation of North Sea gravity data. *In:* Illing, L.V. & Hobson, D. (eds) *Petroleum Geology of the Continental Shelf of North-West Europe*. Institute of Petroleum, London, 65–75.

Duranti, D., Hurst, A., Bell, C., Groves, S. & Hansen, R. 2002. Injected and remobilized sands from the Alba Field (Eocene, UKCS): core and wireline log characteristics. *Petroleum Geoscience*, **8**, 99–107.

Fisher, J.B. & Boles, J.R. 1987. Water–rock interaction in Tertiary sandstones, San Joaquin Basin, California, U.S.A.: diagenetic controls on water composition. *Chemical Geology*, **82**, 83–101.

Fisher, Q.J., Knipe, R.J. & Worden, R.H. 2000. Microstructures of deformed and non-deformed sandstones from the North Sea: implications for the origins of quartz cement in sandstones. *In:* Worden, R.H. & Morad, S. (eds) *Quartz Cementation in Sandstones*. International Association of Sedimentologists, Special Publications, **29**, 129–146.

Friedman, I. & O'Neil, J.R. 1977. Compilation of stable isotope fractionation factors of geochemical interest. *In:* Fleischer, M. (ed.) *Data of Geochemistry*. US Geological Survey, Professional Papers, **440**, 1–12.

Goldstein, R.H. 2001. Fluid inclusions in sedimentary and diagenetic systems. *Lithos*, **55**, 159–193.

Goldstein, R.H. & Reynolds, T.J. 1994. *Systematics of Fluid Inclusions in Diagenetic Minerals*. SEPM Short Course, **31**.

Hillier, S. & Marshall, J.E.A. 1992. Organic maturation, thermal history and hydrocarbon generation in the Orcadian Basin, Scotland. *Journal of the Geological Society, London*, **149**, 491–502.

Huang, Q. 1988. Geometry and tectonic significance of Albian sedimentary dykes in the Sisteron area, SE France. *Journal of Structural Geology*, **10**, 453–462.

Hurst, A. 1982. The clay mineralogy of Jurassic shales from Brora, NE Scotland. *In:* Van Olphen, H. & Veniale, F. (eds) *International Clay Conference 1981*. Developments in Sedimentology, **35**, 677–684.

Jenssen, A.I., Bergslien, D., Rye-Larsen, M. & Lindholm, R.M. 1993. Origin of complex mound geometry of Palaeocene submarine-fan sandstone reservoirs, Balder Field, Norway. *In:* Parker, J.R. (ed.) *Petroleum Geology of Northwest Europe: Proceedings of the 4th Conference*. Geological Society, London, 135–143.

Jolly, R.J.H. & Lonergan, L. 2002. Mechanisms and controls on the formation of sand intrusions. *Journal of the Geological Society, London*, **159**, 605–617.

Jolly, R.J.H., Cosgrove, J.W. & Dewhurst, D.N. 1998. Thickness and spatial distributions of clastic dykes, northwest Sacramento Valley, California. *Journal of Structural Geology*, **20**(12), 1663–1672.

Lonergan, L. & Cartwright, J.A. 1999. Polygonal faults and their influence on deep-water sandstone reservoir geometries, Alba Field, United Kingdom Central North Sea. *AAPG Bulletin*, **83**(3), 410–432.

Macaulay, C.I., Haszeldine, R.S. & Fallick, A.E. 1992. Distribution, chemistry, isotopic composition and origin of diagenetic carbonates: Magnus Sandstone, North Sea. *Journal of Sedimentary Petrology*, **63**(1), 33–43.

Macaulay, C.I., Fallick, A.E., Haszeldine, R.S. & Mcaulay, G.E. 2000. Oil migration makes the difference: regional distribution of carbonate cement $\delta^{13}C$ in northern North Sea Tertiary sandstones. *Clay Minerals*, **35**, 69–76.

Mair, K., Main, I. & Elphick, S. 2000. Sequential growth of deformation bands in the laboratory. *Journal of Structural Geology*, **22**, 25–42.

Marshall, D.J. 1988. *Cathodoluminescence of Geological Materials*. Unwin Hyman, London.

McBride, J.H. 1994. Investigating the crustal structure of a strike-slip step-over zone along the Great Glen fault. *Tectonics*, **13**(5), 1150–1160.

McQuillin, R., Donato, J.A. & Tulstrup, J. 1982. Development of basins in the Inner Moray Firth and the North Sea by crustal extension and dextral displacement of the Great Glen Fault. *Earth and Planetary Science Letters*, **60**, 127–139.

Morad, S. 1998. Carbonate cementation in sandstones: distribution patterns and geochemical evolution. *In:* Morad, S. (ed.) *Carbonate Cementation in Sandstones*. International Association of Sedimentologists, Special Publications, **26**, 1–26.

Murchison, R.I. 1827. Supplementary remarks on the Oolitic Series in the Counties of Sutherland and Ross, and in the Hebrides. *Transactions of the Geological Society*, **2**(ii), 353.

Newsome, J.F. 1903. Clastic dikes. *Geological Society of America Bulletin*, **14**, 227–268.

Pearson, M.J. & Watkins, D. 1983. Organofacies and early maturation effects in Upper Jurassic sediments from the Inner Moray Firth Basin, North Sea. *In:* Brooks, J. (ed.) *Petroleum Geochemistry and Exploration of Europe*. Geological Society, London, 147–158.

Pickering, K.T. 1984. The Upper Jurassic Boulder Beds and related deposits: a fault-controlled submarine slope, NE Scotland. *Journal of the Geological Society, London*, **141**, 357–374.

Richter, D. 1966. On the New Red Sandstone Neptunian Dykes of the Tor Bay Area (Devonshire). *Proceedings of the Geological Association*, **77**(2), 172–186.

Roberts, A.H. 1989. Fold and thrust structures in the Kintradwell Boulder Beds Moray Firth. *Scottish Journal of Geology*, **25**, 173–186.

Roberts, A.M., Badley, M.E., Price, J.D. & Huck, I.W. 1990. The structural history of a transtensional basin: Inner Moray Firth, NE Scotland. *Journal of the Geological Society, London*, **147**, 87–103.

Roedder, E. 1984. *Fluid Inclusions*. Mineralogical Society of America, Reviews in Mineralogy, **xx**.

Shackleton, N.J. & Kennett, J.P. 1975. Palaeotemperature history of the Cenozoic and initiation of Antarctic glaciation: oxygen and carbon isotope analyses in DSDP sites 277. *In:* Editor, A. (ed.) *Deep Sea Drilling Project, Initial Reports, 29*. US Government Printing Office, Washington, DC, 743–755.

Speight, J.M. & Mitchell, J.G. 1979. The Permo-Carboniferous dyke-swarm of northern Argyll and its bearing on dextral displacement of the Great Glen Fault. *Journal of the Geological Society, London*, **136**, 3–11.

Thomson, K. & Underhill, J.R. 1993. Controls on the development and evolution of structural styles in the Inner Moray Firth Basin. *In:* Parker, J.R. (ed.) *Petroleum Geology of Northwest Europe: Proceedings of the 4th Conference*. Geological Society, London, 1167–1178.

Trewin, N.H. & Hurst, A. 1993. *Geology of East Sutherland and Caithness*. Geological Society of Aberdeen, Aberdeen.

Underhill, J.R. & Brodie, J.A. 1993. Structural geology of Easter Ross, Scotland: implications for movement on the Great Glen fault zone. *Journal of the Geological Society, London*, **150**, 515–527.

Van den Kerkhof, A.M. & Hein, U.F. 2001. Fluid inclusion petrography. *Lithos*, **55**, 27–47.

Waterston, C.D. 1950. Note on the sandstone injections of Eathie Haven, Cromarty. *Geological Magazine*, **87**, 133–139.

Waterston, C.D. 1951. The stratigraphy and palaeontology of the Jurassic rocks of Eathie (Cromarty). *Transactions of the Royal Society of Edinburgh*, **62**, 33–51.

Watson, R.S., Trewin, N.H. & Fallick, A.E. 1995. The formation of carbonate cements in the Forth and Balmoral fields, northern North Sea: a case for biodegradation, carbonate cementation and oil leakage during early burial. *In:* Hartley, A.J. & Prosser, D.J. (eds) *Characterization of Deep Marine Clastic Systems*. Geological Society, London, Special Publications, **94**, 177–200.

Wilkinson, J.J., Lonergan, L., Fairs, T. & Herrington, R.J. 1998. Fluid inclusion constraints on conditions and timing of hydrocarbon migration and quartz cementation in Brent Group reservoir sandstones, Columba Terrace, northern North Sea. *In:* Parnell, J. (ed.) *Dating and Duration of Fluid Flow and Fluid–Rock Interaction*. Geological Society, London, Special Publications, **144**, 69–89.

Winslow, M.A. 1983. Clastic dike swarms and the structural evolution of the foreland fold and thrust belt of the southern Andes. *Geological Society of America Bulletin*, **94**, 1073–1080.

Zhang, Y. & Dawe, R. 1998. The kinetics of calcite precipitation from a high salinity water. *Applied Geochemistry*, **13**, 177–184.

Received 1 July 2002; revised typescript accepted 5 June 2003.
Scientific editing by Joe Macquaker